

Double-integrator multirobot control with uncoupled dynamics for transport of deformable objects

Rafael Herguedas^{1,2}, Miguel Aranda¹, Gonzalo López-Nicolás¹, Carlos Sagüés¹ and Youcef Mezouar³

Abstract—We present a formation controller for a team of mobile robots, modelled with double-integrator dynamics, to manipulate deformable objects grasped around their contour. The manipulation task is defined as reaching a target configuration consisting of a desired shape, scale, position and orientation of the formation in 2D, while preserving the integrity of the object. We provide a set of controllers designed to allow the uncoupled control of the variables that define the task. The formal analysis of the controllers is covered in depth in terms of uncoupling, stability and convergence to the equilibrium state. Besides, we include control barrier functions to enforce safety constraints relevant to the task, i.e., collision and excessive stretching avoidance. The performance of the method is illustrated in simulations and in real experiments.

Index Terms—Multi-Robot Systems, Mobile Manipulation, Formation Control, Deformable Objects.

I. INTRODUCTION

DEFORMABLE objects need to be handled in diverse environments and tasks [1]. Spreading and folding cloth in domestic contexts, for instance, may involve the transport and simultaneous control of the shape of large deformable objects. In industrial sectors, such as the textile and the footwear ones, large deformable materials (e.g. fabric, leather and foam sheets) are transported and progressively transformed across different workstations. The benefits of automatizing this kind of manipulation tasks are evident, as well as the complexity of developing such autonomous systems. Multiple manipulators to handle deformable objects are commonly considered [2], [3]. This applies specially to large, fragile and heavy objects or

Manuscript received: May, 12, 2023; Revised July, 9, 2023; Accepted September, 9, 2023.

This paper was recommended for publication by Editor Aniket Bera upon evaluation of the Associate Editor and Reviewers' comments. This work was supported via projects PID2021-124137OB-I00, TED2021-130224B-I00 funded by MCIN/AEI/10.13039/501100011033, by ERDF A way of making Europe and by the European Union NextGenerationEU/PRTR, projects DGA T45-23R and T73-23R by Gobierno de Aragón and project SOFTMANBOT (European Union's Horizon 2020 Research and Innovation Programme, under Grant agreement No 869855). R. Herguedas was partially supported by the EU through the European Social Fund (ESF) "Construyendo Europa desde Aragón". M. Aranda was supported via a María Zambrano fellowship funded by the Spanish Ministry of Universities and by the European Union-NextGenerationEU.

¹R. Herguedas, M. Aranda, G. López-Nicolás and C. Sagüés are with Instituto de Investigación en Ingeniería de Aragón (I3A), Universidad de Zaragoza, Spain {rherguedas, miguel.aranda, gonlopez, csagues}@unizar.es

²R. Herguedas is also with Instituto Tecnológico de Aragón, Zaragoza, Spain rherguedas@itainnova.es

³Y. Mezouar is with CNRS, Clermont Auvergne INP, Institut Pascal, Université Clermont Auvergne, F-63000 Clermont-Ferrand, France youcef.mezouar@sigma-clermont.fr

if the task requires great dexterity. Formation control methods are a suitable option to manipulate deformable objects with multirobot systems, since accurate and tightly coordinated motions are needed.

1) *Related work*: Formation control methods can be classified depending on the dynamic model of the robots they consider. Single-integrator dynamics has been widely adopted [4], [5]. Other studies in this area develop methods for robots with higher-order models. Lin *et al.* propose an affine formation controller for robots with single-integrator and second-order dynamics [6]. A different study by Fathian *et al.* proposes a distributed control strategy where the robots are modelled with single-integrator and higher-order holonomic dynamics [7]. Steering robots with single-integrator, double integrator and unicycle models to a desired geometric pattern is the goal of the work proposed by Zhao [8]. Another study by Zhao *et al.* shows an approach for coordinating multiple robots with motion constraints, in two and three dimensions by means of a gradient-descent control law [9]. Unlike these prior formation controllers for robots with high-order dynamics, here we consider deformable objects, and the constraints their behaviour imposes, in our formulation. We also leverage Control Barrier Functions (CBFs) [10], which have been previously exploited, e.g., for collision avoidance in multirobot systems [11] or robotic grasping [12]. Here, we apply CBFs to avoid collisions and object overstretching in the transport of deformable objects.

Different works have tackled tasks where deformable objects are manipulated. In this area, a method based on the As-Rigid-As-Possible (ARAP) model [13], where previous information about the mechanical properties of the object is not needed, exploits shape servoing [14]. Planning strategies have also been developed for manipulating deformable objects with multiple manipulators [15], [16]. Alternating planning and control by means of a deadlock prediction system is another approach to solve the problem of manipulating deformable objects [17]. The task of transporting a rigid object with a deformable sheet, held by multiple mobile manipulators, has also received attention in the last years [18], [19]. However, the uncoupled control of the variables defining the configuration of the manipulators has not been studied by these works. Finally, previous systems for transporting deformable objects to goal configurations have been proposed [20], [21]. In the first work [20], smooth admissible trajectories are followed for preserving the integrity of the object, but collision avoidance is not tackled. In the second work [21], a Deformable Bounding Box model (DBB) is presented where, in contrast to the present strategy, the configuration parameters are only the

dimensions, rotation and position of the DBB, and the stability and convergence of the method are not formally analyzed.

2) *Contributions:* We build our new developments upon a previous study [22], where we designed a controller with terms for each formation variable (shape, scale, position and orientation). We augmented that controller with a set of CBFs to avoid overstretching, robot-to-robot, robot-to-obstacle and object-to-obstacle collisions [22]. The main contributions presented here, with respect to the previous studies, are a new control term that guarantees full uncoupling between the controlled formation variables, a comprehensive formal analysis of uncoupling, stability and convergence of the proposal and new simulations and experimental results, that illustrate the performance of our method.

3) *Problem statement:* Let us consider a deformable object that is carried by a formation of N robots in \mathbb{R}^2 . The object is connected to the robots by a set of points $\mathbf{P} = [\mathbf{p}_1, \mathbf{p}_2, \dots, \mathbf{p}_N] \in \mathbb{R}^{2 \times N}$, where $\mathbf{p}_i = [p_{ix}, p_{iy}]^\top$, $i = 1, \dots, N$ denotes the center of robot i . We model the robot-object links as free-rotating joints, since this allows the object's shape to adapt more easily to the robot team's configuration. The formation centroid is $\mathbf{g} = \frac{1}{N} \mathbf{P} \mathbf{1}_N$, with $\mathbf{1}_N$ being a column vector of N ones. s and θ denote the scale and orientation of the formation, respectively. We consider the double-integrator model to describe the robots' dynamics:

$$\begin{bmatrix} \dot{\mathbf{p}}_i \\ \ddot{\mathbf{p}}_i \end{bmatrix} = \begin{bmatrix} \mathbf{0} & \mathbf{I}_{2 \times 2} \\ \mathbf{0} & \mathbf{0} \end{bmatrix} \begin{bmatrix} \mathbf{p}_i \\ \dot{\mathbf{p}}_i \end{bmatrix} + \begin{bmatrix} \mathbf{0} \\ \mathbf{I}_{2 \times 2} \end{bmatrix} \mathbf{u}_i, \quad (1)$$

where $\mathbf{x}_i = [\mathbf{p}_i^\top, \dot{\mathbf{p}}_i^\top]^\top$ is the state of robot i and $\mathbf{u}_i = [u_{ix}, u_{iy}]^\top$, $i = 1, \dots, N$ is its control input.

The goal task consists in driving the deformable object to a target configuration, understood as a specific combination of shape, scale, position and orientation of the robotic formation. We adopt a strategy to solve this problem such that the configuration of the object is not controlled explicitly. Instead, the proposed controllers act over the formation of robots that manipulate the object. Our method is especially suited for highly deformable objects, such as cloths or foam parts. The reason is that their deformability allows the structure of these objects to follow closely the shape of the formation. The goal configuration of the formation is encoded by a set of variables. We define the desired shape of the formation as the matrix $\mathbf{P}_d = [\mathbf{p}_{d1}, \mathbf{p}_{d2}, \dots, \mathbf{p}_{dN}] \in \mathbb{R}^{2 \times N}$, where $\mathbf{p}_{di} = [p_{dix}, p_{diy}]^\top$, $i = 1, \dots, N$ are the positions of the robots in the desired shape. Using the desired formation scale s_d and the desired formation orientation θ_d , we can express the target configuration as

$$\mathbf{P}_T = s_d \mathbf{R}_d(\theta_d)(\mathbf{P}_d - \mathbf{g}_d \mathbf{1}_N^\top) + \mathbf{g}_d \mathbf{1}_N^\top, \quad (2)$$

where $\mathbf{R}_d(\theta_d) \in SO(2)$. Without loss of generality we consider that the desired shape is centered around the desired formation centroid $\mathbf{g}_d = \frac{1}{N} \mathbf{P}_d \mathbf{1}_N$, and $\theta_d = 0$.

II. FORMATION CONTROL FOR ROBOTS WITH DOUBLE-INTEGRATOR DYNAMICS

We present our proposed controllers next. We design them so that each term is focused on a specific variable of interest.

A. Shape control

First, we will describe the controller we propose for achieving the desired shape of the formation. This controller is based on a cost function that defines the shape error of the robotic formation relative to the desired shape [4]:

$$\gamma = \frac{1}{2} \|\mathbf{P}_b - \mathbf{H} \mathbf{P}_{db}\|_F^2 = \frac{1}{2} \text{tr} \left((\mathbf{P}_b - \mathbf{H} \mathbf{P}_{db})^\top (\mathbf{P}_b - \mathbf{H} \mathbf{P}_{db}) \right), \quad (3)$$

where $\|\cdot\|_F$ denotes the Frobenius norm and tr denotes the trace. The matrix $\mathbf{H} \in \mathbb{R}^{2 \times 2}$ in (3), assumed $\neq \mathbf{0}$, is defined as $\mathbf{H} = [(h_1, h_2)^\top, (-h_2, h_1)^\top]$, where

$$h_1 = \frac{\text{tr}(\mathbf{P}_b \mathbf{P}_{db}^\top)}{\text{tr}(\mathbf{P}_b \mathbf{P}_{db}^\top)}, \quad h_2 = \frac{\text{tr}(\mathbf{P}_b (\mathbf{S} \mathbf{P}_{db})^\top)}{\text{tr}(\mathbf{P}_b \mathbf{P}_{db}^\top)}, \quad (4)$$

and $\mathbf{S} = [(0, 1)^\top, (-1, 0)^\top]$. The matrix \mathbf{H} aligns the matrices \mathbf{P}_b and \mathbf{P}_{db} by performing rotation and uniform scaling. \mathbf{P}_b and \mathbf{P}_{db} represent, respectively, the current and desired shape of the formation with zero centroid, and are defined as

$$\mathbf{P}_b = \mathbf{P} - \mathbf{g} \mathbf{1}_N^\top = \mathbf{P} \mathbf{K}_b, \quad (5)$$

$$\mathbf{P}_{db} = \mathbf{P}_d - \mathbf{g}_d \mathbf{1}_N^\top = \mathbf{P}_d \mathbf{K}_b, \quad (6)$$

with $\mathbf{K}_b = \mathbf{I}_{N \times N} - (1/N) \mathbf{1}_N \mathbf{1}_N^\top$. Observe that \mathbf{K}_b is a centering matrix that satisfies $\mathbf{K}_b^\top = \mathbf{K}_b$, $\mathbf{K}_b \mathbf{1}_N = \mathbf{0}$ and $\mathbf{K}_b \mathbf{K}_b = \mathbf{K}_b$. We also define $\mathbf{E}_\gamma \in \mathbb{R}^{2 \times N}$ as the matrix of the position errors relative to the desired shape:

$$\mathbf{E}_\gamma = \mathbf{P}_b - \mathbf{H} \mathbf{P}_{db}. \quad (7)$$

Therefore, we can also express γ as follows:

$$\gamma = \frac{1}{2} \text{tr}(\mathbf{E}_\gamma^\top \mathbf{E}_\gamma). \quad (8)$$

Then, we build the controller from (3) as the linear combination of the negative gradient of γ and the time derivative of the negative gradient of γ :

$$\begin{aligned} \mathbf{U}_H &= -k_{1H} \nabla_{\mathbf{P}} \gamma - k_{2H} \frac{d(\nabla_{\mathbf{P}} \gamma)}{dt} = \\ &= k_{1H} (\mathbf{H} \mathbf{P}_{db} - \mathbf{P}_b) + k_{2H} (\dot{\mathbf{H}} \mathbf{P}_{db} - \dot{\mathbf{P}}_b), \end{aligned} \quad (9)$$

being k_{1H} and k_{2H} positive control gains. Inspired by the control scheme proposed by Fathian *et al.* [7, eq. (22)], this controller aims at optimally driving the formation so that the cost function and its time derivative are reduced. This implies a direct reduction of the difference in shape between \mathbf{P}_b and \mathbf{P}_{db} . Due to the fact that there is no direct control over the transition from \mathbf{P}_b and \mathbf{P}_{db} , if the difference between them is large, \mathbf{U}_H may temporarily reorder the robots around the object. For example, if the formation consists of three robots following a clockwise ordering $\{1, 2, 3\}$, \mathbf{U}_H may modify the sequence to $\{2, 1, 3\}$ or $\{1, 3, 2\}$. This reordering could fold or twist the object that is being manipulated by the formation, causing undesired deformations or structural damage. For avoiding these undesired effects, we formulate a correcting term

$$\mathbf{U}_G = k_{1G} (\mathbf{P}_b \mathbf{P}_{db}^+ \mathbf{P}_{db} - \mathbf{P}_b) + k_{2G} (\dot{\mathbf{P}}_b \mathbf{P}_{db}^+ \mathbf{P}_{db} - \dot{\mathbf{P}}_b), \quad (10)$$

where $\mathbf{P}_{db}^+ = \mathbf{P}_{db}^\top (\mathbf{P}_{db} \mathbf{P}_{db}^\top)^{-1}$ represents the Moore-Penrose pseudoinverse of matrix \mathbf{P}_{db} and k_{1G} and k_{2G} are positive

control gains. This term is based on an optimal affine transformation that aligns \mathbf{P}_{db} with \mathbf{P}_b in a least-squares manner. \mathbf{U}_G steers the system towards $\mathbf{P}_b \mathbf{P}_{db}^+ \mathbf{P}_{db}$, which is the optimal affine deformation of \mathbf{P}_{db} . We denote by $\mathbf{G} \in \mathbb{R}^{2 \times 2}$ the matrix that expresses this deformation:

$$\mathbf{G} = \mathbf{P}_b \mathbf{P}_{db}^+. \quad (11)$$

Therefore, \mathbf{U}_G can also be expressed as

$$\mathbf{U}_G = k_{1G}(\mathbf{GP}_{db} - \mathbf{P}_b) + k_{2G}(\dot{\mathbf{GP}}_{db} - \dot{\mathbf{P}}_b). \quad (12)$$

For numerical reasons, \mathbf{U}_G is compatible with desired shapes different from a straight line, and it limits the movements of the robots to those that produce the deformation modes of stretch and shear [4]. Note that it is still possible to manipulate rope-like objects in straight-line configurations with the method we propose, and this control term would be unnecessary. We define another variable to use in our analysis: $\mathbf{E}_{GH} \in \mathbb{R}^{2 \times N}$, which measures the difference between the configurations that result from applying the two transformation matrices \mathbf{G} and \mathbf{H} :

$$\mathbf{E}_{GH} = \mathbf{GP}_{db} - \mathbf{HP}_{db}. \quad (13)$$

We combine the previous controllers in

$$\mathbf{U}_\gamma = \alpha_H \mathbf{U}_H + \alpha_G \mathbf{U}_G. \quad (14)$$

The positive control weights α_H and α_G regulate the contribution of each term, so that α_G should be greater than α_H if there is a large difference between \mathbf{P}_b and \mathbf{P}_{db} . Otherwise, the convergence speed can be increased with a greater value of α_H . As shown in Section IV, this shape controller steers γ to zero. This makes the team acquire the shape of \mathbf{P}_d .

B. Scale control

Scaling the shape of the formation consists in uniformly driving the robots closer or further to the formation centroid. Just like \mathbf{U}_γ , this process creates deformations over the object, since it modifies the relative positions of the robots that grasp it. The formation scale can be obtained as $s = \|\mathbf{H}\|_2$. For getting $s = s_d$, we propose the controller

$$\mathbf{U}_s = -k_{1s}e_s(1/s)\mathbf{HP}_{db} - k_{2s}\dot{\mathbf{P}}_b, \quad (15)$$

where $e_s = s - s_d$ represents the scale error and k_{1s} and k_{2s} are positive control gains. This controller produces a uniform scaling of the goal shape \mathbf{HP}_{db} , which is proportional to the scale error and the velocity of the robots.

Assumption 1. *We assume scale $s > 0$ initially ($t=0$). As we will show later, we can control the dynamics of s independently from the rest of the variables with \mathbf{U}_s . Therefore, by selecting the control gains appropriately, we can guarantee $s > 0, \forall t \geq 0$, with a monotonic convergence to s_d . Note that this requirement is necessary for the orientation of the formation θ to be defined at all times.*

C. Translation and rotation control

Translation and rotation of the robotic formation consist in driving the formation rigidly from one place to another and rotating the shape around the formation centroid, respectively. We can obtain the orientation of the formation as $\theta = \text{atan2}(h_2, h_1) \in (-\pi, \pi]$, where the atan2 operator represents the four quadrant inverse tangent. Note that θ can be assumed to always remain differentiable in terms of h_1 and h_2 , as done in [4]. The controllers we apply to get these transformations are

$$\mathbf{U}_g = -k_{1g}\mathbf{e}_g \mathbf{1}_N^\top - k_{2g}\dot{\mathbf{P}}_b, \quad (16)$$

$$\mathbf{U}_\theta = -k_{1\theta}e_\theta \mathbf{SHP}_{db} - k_{2\theta}\dot{\mathbf{P}}_b, \quad (17)$$

with $\mathbf{e}_g = \mathbf{g} - \mathbf{g}_d$ being the translation error, $e_\theta = \theta - \theta_d$ being the orientation error, and k_{1g} , k_{2g} , $k_{1\theta}$ and $k_{2\theta}$ being positive control gains.

D. Full formation controller

The full formation controller consists in a linear combination of the shape, scale, translation and rotation controllers for robots with double-integrator dynamics ($\mathbf{U}_\gamma + \mathbf{U}_s + \mathbf{U}_g + \mathbf{U}_\theta$). This control law provides suitable performance. However, when using it, the dynamic evolution of the variables s and θ is coupled. The underlying reason for this coupling can be found by computing the dynamics of these variables as a function of h_1 and h_2 . Using standard manipulations and also the facts that $h_1 = s \cos \theta$ and $h_2 = s \sin \theta$, we get:

$$\dot{s} = \frac{h_1 \dot{h}_1 + h_2 \dot{h}_2}{s}, \quad \ddot{s} = \frac{h_1 \ddot{h}_1 + h_2 \ddot{h}_2}{s} + \dot{\theta}^2 s. \quad (18)$$

$$\dot{\theta} = \frac{h_1 \dot{h}_2 - h_2 \dot{h}_1}{s^2}, \quad \ddot{\theta} = \frac{h_1 \ddot{h}_2 - h_2 \ddot{h}_1}{s^2} - \frac{2\dot{s}\dot{\theta}}{s}. \quad (19)$$

The second addends in the second-order time derivatives of s and of θ cause the coupling. Specifically, it turns out that s is not invariant when using \mathbf{U}_θ , as we analyze in Section III. To remove this coupling, we define a control term \mathbf{U}_u having the following form:

$$\mathbf{U}_u = -\dot{\theta}^2 \mathbf{HP}_{db} + (2\dot{s}\dot{\theta}/s)\mathbf{SHP}_{db}. \quad (20)$$

The first addend of \mathbf{U}_u aims at modifying the dynamics of \mathbf{U}_s , while the second one does that for \mathbf{U}_θ . The full control law we apply is, then:

$$\mathbf{U} = \mathbf{U}_\gamma + \mathbf{U}_g + \mathbf{U}_s + \mathbf{U}_\theta + \mathbf{U}_u. \quad (21)$$

As we show in Section IV, \mathbf{U}_u will cancel out the coupled dynamic terms. Then, under the control (21), we will obtain uncoupled dynamics for all the variables (γ , θ , \mathbf{g} and s).

III. INVARIANCE AND UNCOUPLING UNDER THE PROPOSED CONTROL TERMS

Uncoupling is a desired property for the proposed controller. When it applies, it is possible to control each variable independently. This results in flexible solutions, which can be adapted to different manipulation tasks. It is also possible to study other control properties of every term separately (e.g., stability),

if uncoupling between them exists. To study uncoupling, we analyze in this section the invariance of each variable (γ , \mathbf{g} , θ and s) under the proposed controllers. Note that we analyze the role of \mathbf{U}_u to fully uncouple the control of the formation variables in Section IV. In our analysis we will assume the system is at rest initially, i.e., $\dot{\mathbf{P}}(t = 0) = \mathbf{0}$. At the end of this section (Remark 1), we will summarize the results of our invariance study.

Proposition 1. *The formation variable γ is invariant under \mathbf{U}_g , \mathbf{U}_s and \mathbf{U}_θ .*

Proof. We will use the time derivative of γ , which has the following expression:

$$\dot{\gamma} = \text{tr}\left(\mathbf{P}_b^\top \dot{\mathbf{P}}_b - \mathbf{P}_{db}^\top \mathbf{H}^\top \dot{\mathbf{P}}_b - \mathbf{P}_{db}^\top \dot{\mathbf{H}}^\top \mathbf{P}_b + \mathbf{P}_{db}^\top \dot{\mathbf{H}}^\top \mathbf{H} \mathbf{P}_{db}\right). \quad (22)$$

We will now find a simpler expression for this derivative. First, we know from Aranda *et al.* [4] that

$$\mathbf{H} \mathbf{P}_{db} = h_1 \mathbf{P}_{db} + h_2 \mathbf{S} \mathbf{P}_{db}, \quad (23)$$

and hence

$$\dot{\mathbf{H}} \mathbf{P}_{db} = \dot{h}_1 \mathbf{P}_{db} + \dot{h}_2 \mathbf{S} \mathbf{P}_{db}. \quad (24)$$

Using these two identities, the definitions (4), and applying the property $\text{tr}((\mathbf{S}\mathbf{A})\mathbf{A}^\top) = \text{tr}((\mathbf{S}\mathbf{A})^\top \mathbf{A}) = 0$ with $\mathbf{A} \in \mathbb{R}^{2 \times N}$ for $\mathbf{A} = \mathbf{P}_{db}$, we find the identity

$$\begin{aligned} \text{tr}(\mathbf{P}_{db}^\top \dot{\mathbf{H}}^\top \mathbf{H} \mathbf{P}_{db}) &= \\ &= \text{tr}\left((\dot{h}_1 \mathbf{P}_{db} + \dot{h}_2 \mathbf{S} \mathbf{P}_{db})^\top (h_1 \mathbf{P}_{db} + h_2 \mathbf{S} \mathbf{P}_{db})\right) \\ &= h_1 \dot{h}_1 \text{tr}(\mathbf{P}_{db} \mathbf{P}_{db}^\top) + h_2 \dot{h}_2 \text{tr}(\mathbf{P}_{db}^\top \mathbf{S}^\top \mathbf{S} \mathbf{P}_{db}) \\ &= h_1 \text{tr}(\dot{\mathbf{P}}_b^\top \mathbf{P}_{db}) + h_2 \text{tr}(\dot{\mathbf{P}}_b^\top \mathbf{S} \mathbf{P}_{db}) = \text{tr}(\mathbf{P}_{db}^\top \mathbf{H}^\top \dot{\mathbf{P}}_b). \end{aligned} \quad (25)$$

Using this on (22), we reach the simpler expression

$$\dot{\gamma} = \text{tr}(\mathbf{P}_b^\top \dot{\mathbf{P}}_b - \mathbf{P}_{db}^\top \dot{\mathbf{H}}^\top \mathbf{P}_b). \quad (26)$$

We present the study for each controller next.

1) **γ is invariant under \mathbf{U}_g .** With $\ddot{\mathbf{P}} = \mathbf{U}_g$, we have $\ddot{\mathbf{P}}_b = \dot{\mathbf{P}} \mathbf{K}_b = \mathbf{U}_g \mathbf{K}_b = -k_{1g} \mathbf{e}_g \mathbf{1}_N^\top \mathbf{K}_b - k_{2g} \dot{\mathbf{P}}_b$. Since $\mathbf{1}_N^\top \mathbf{K}_b = (\mathbf{K}_b \mathbf{1}_N)^\top = \mathbf{0}$ and assuming initial rest (i.e., $\dot{\mathbf{P}}(t = 0) = \mathbf{0}$), we see that $\ddot{\mathbf{P}}_b = \dot{\mathbf{P}}_b = \mathbf{0} \forall t$. Hence, $\ddot{\mathbf{H}} = \dot{\mathbf{H}} = \mathbf{0} \forall t$. Substituting $\dot{\mathbf{P}}_b = \mathbf{0}$ and $\dot{\mathbf{H}} = \mathbf{0}$ in (26), we obtain $\dot{\gamma} = 0$.

2) **γ is invariant under \mathbf{U}_s .** We will show that, under \mathbf{U}_s ,

$$\text{tr}(\mathbf{P}_b^\top \dot{\mathbf{P}}_b) = \text{tr}(\mathbf{P}_{db}^\top \dot{\mathbf{H}}^\top \mathbf{P}_b), \quad (27)$$

which implies, from (26), the invariance of γ . Notice

$$\ddot{\mathbf{P}}_b = \mathbf{U}_s \mathbf{K}_b = -k_{1s}(1 - s_d/s) \mathbf{H} \mathbf{P}_{db} - k_{2s} \dot{\mathbf{P}}_b. \quad (28)$$

We can use this to compute

$$\begin{aligned} \ddot{h}_1 &= \text{tr}\left((-k_{1s}(1 - s_d/s) \mathbf{H} \mathbf{P}_{db} - k_{2s} \dot{\mathbf{P}}_b) \mathbf{P}_{db}^\top\right) / \text{tr}(\mathbf{P}_{db} \mathbf{P}_{db}^\top) \\ &= -k_{1s}(1 - s_d/s) h_1 - k_{2s} \dot{h}_1, \end{aligned} \quad (29)$$

where we used $h_1 = \text{tr}(\mathbf{H} \mathbf{P}_{db} \mathbf{P}_{db}^\top) / \text{tr}(\mathbf{P}_{db} \mathbf{P}_{db}^\top)$ [4]. Since an analogous equation holds for \ddot{h}_2 , we get

$$\ddot{\mathbf{h}} + k_{2s} \dot{\mathbf{h}} + k_{1s} (1 - s_d/\|\mathbf{h}\|) \mathbf{h} = \mathbf{0}. \quad (30)$$

where we defined $\mathbf{h} = [h_1, h_2]^\top$, with $\|\mathbf{h}\| = s$. Starting from rest ($\mathbf{h}(t = 0) = \mathbf{0}$), we see that the dynamics of this equation must remain proportional to \mathbf{h} ; i.e., $\mathbf{h}(t) = \kappa(t)\mathbf{h}(t = 0)$ with $\kappa(t)$ being a scalar. Note that $\kappa(t) \neq 0$ because $\kappa(t) = 0$ would imply $s(t) = 0$, which is ruled out by Assumption 1. We can directly write for \mathbf{H} :

$$\mathbf{H}(t) = \kappa(t) \mathbf{H}(0). \quad (31)$$

where $\mathbf{H}(0)$ is \mathbf{H} at time zero. By reorganizing (28) and substituting (31), we get

$$\ddot{\mathbf{P}}_b + k_{2s} \dot{\mathbf{P}}_b + k_{1s} (1 - s_d/s) \kappa(t) \mathbf{H}(0) \mathbf{P}_{db} = \mathbf{0}. \quad (32)$$

Defining a constant matrix $\mathbf{P}_{dbo} = \mathbf{H}(0) \mathbf{P}_{db}$, we express the above as a first order differential equation in $\dot{\mathbf{P}}_b$:

$$\ddot{\mathbf{P}}_b + k_{2s} \dot{\mathbf{P}}_b + \kappa_1(t) \mathbf{P}_{dbo} = \mathbf{0}, \quad (33)$$

for some scalar $\kappa_1(t)$. Starting from rest ($\dot{\mathbf{P}}_b(t = 0) = \mathbf{0}$), the solution to this equation has the form

$$\dot{\mathbf{P}}_b = \kappa_2(t) \mathbf{P}_{dbo} = \kappa_2(t) \mathbf{H}(0) \mathbf{P}_{db} = \mu(t) \mathbf{H} \mathbf{P}_{db}, \quad (34)$$

with $\kappa_2(t)$, $\mu(t)$ scalars such that $\mu(t) = \kappa_2(t)/\kappa(t)$. Hence

$$\dot{h}_1 = \frac{\text{tr}(\dot{\mathbf{P}}_b \mathbf{P}_{db}^\top)}{\text{tr}(\mathbf{P}_{db} \mathbf{P}_{db}^\top)} = \frac{\mu(t) \text{tr}(\mathbf{H} \mathbf{P}_{db} \mathbf{P}_{db}^\top)}{\text{tr}(\mathbf{P}_{db} \mathbf{P}_{db}^\top)} = \mu(t) h_1, \quad (35)$$

where we have used $\text{tr}(\mathbf{H} \mathbf{P}_{db} \mathbf{P}_{db}^\top) = \text{tr}(\mathbf{P}_b \mathbf{P}_{db}^\top)$, which can be deduced from (23). Note $\dot{h}_2 = \mu(t) h_2$ holds too. Using this, (34) and (23) in (27) we get:

$$\begin{aligned} \text{tr}(\mathbf{P}_b^\top \dot{\mathbf{P}}_b) &= \mu(t) \text{tr}(\mathbf{P}_b^\top (\mathbf{H} \mathbf{P}_{db})) \\ &= \mu(t) h_1 \text{tr}(\mathbf{P}_b^\top \mathbf{P}_{db}) + \mu(t) h_2 \text{tr}(\mathbf{P}_b^\top \mathbf{S} \mathbf{P}_{db}) \\ &= \dot{h}_1 \text{tr}(\mathbf{P}_b^\top \mathbf{P}_{db}) + \dot{h}_2 \text{tr}(\mathbf{P}_b^\top \mathbf{S} \mathbf{P}_{db}) \\ &= \text{tr}(\mathbf{P}_b^\top \dot{\mathbf{H}} \mathbf{P}_{db}) = \text{tr}(\mathbf{P}_{db}^\top \dot{\mathbf{H}}^\top \mathbf{P}_b). \end{aligned} \quad (36)$$

Therefore, (27) holds. Hence, γ is invariant under \mathbf{U}_s .

3) **γ is invariant under \mathbf{U}_θ .** By recovering once again the expression for \ddot{h}_1 and substituting $\ddot{\mathbf{P}}_b = \mathbf{U}_\theta \mathbf{K}_b$, we get

$$\begin{aligned} \ddot{h}_1 &= \left(\text{tr}(\mathbf{P}_{db} \mathbf{P}_{db}^\top)\right)^{-1} \text{tr}\left((-k_{1\theta} e_\theta \mathbf{S} \mathbf{H} \mathbf{P}_{db} - k_{2\theta} \dot{\mathbf{P}}_b) \mathbf{P}_{db}^\top\right) \\ &= -k_{1\theta} e_\theta \left(\text{tr}(\mathbf{P}_{db} \mathbf{P}_{db}^\top)\right)^{-1} \text{tr}\left(\mathbf{S}(h_1 \mathbf{P}_{db} + h_2 \mathbf{S} \mathbf{P}_{db}) \mathbf{P}_{db}^\top\right) \\ &\quad - k_{2\theta} \dot{h}_1 = k_{1\theta} e_\theta h_2 - k_{2\theta} \dot{h}_1, \end{aligned} \quad (37)$$

where we used that $\mathbf{S} \mathbf{S} = -\mathbf{I}_{2 \times 2}$. Similarly, we find $\ddot{h}_2 = -k_{1\theta} e_\theta h_1 - k_{2\theta} \dot{h}_2$. Then, we can obtain:

$$\ddot{\mathbf{H}} + k_{2\theta} \dot{\mathbf{H}} + k_{1\theta} e_\theta \mathbf{S} \mathbf{H} = \mathbf{0}. \quad (38)$$

On the other hand, we can rewrite $\mathbf{U}_\theta \mathbf{K}_b$ as

$$\ddot{\mathbf{P}}_b + k_{2\theta} \dot{\mathbf{P}}_b + k_{1\theta} e_\theta \mathbf{S} \mathbf{H} \mathbf{P}_{db} = \mathbf{0}. \quad (39)$$

If we post-multiply (38) by \mathbf{P}_{db} and we subtract the result from (39), we obtain

$$(\ddot{\mathbf{P}}_b - \ddot{\mathbf{H}} \mathbf{P}_{db}) + k_{2\theta}(\dot{\mathbf{P}}_b - \dot{\mathbf{H}} \mathbf{P}_{db}) = \mathbf{0}. \quad (40)$$

Assuming the system initially at rest, i.e., $\dot{\mathbf{P}}_b - \dot{\mathbf{H}} \mathbf{P}_{db} = \mathbf{0}$ at $t = 0$, clearly $\ddot{\mathbf{P}}_b = \ddot{\mathbf{H}} \mathbf{P}_{db}$ and $\dot{\mathbf{P}}_b = \dot{\mathbf{H}} \mathbf{P}_{db} \forall t$. Then, the equality (27) is satisfied and (26) equals zero. Hence, $\dot{\gamma} = 0$. This indicates that γ is invariant under \mathbf{U}_θ . \square

Proposition 2. *The formation variable \mathbf{g} is invariant under \mathbf{U}_γ , \mathbf{U}_s and \mathbf{U}_θ .*

Proof. Notice that every addend in \mathbf{U}_γ , \mathbf{U}_s and \mathbf{U}_θ can be expressed as $\mathbf{U}_i \mathbf{K}_b$. Therefore, for every such addend the dynamics of \mathbf{g} is $\dot{\mathbf{g}} = \frac{1}{N} \ddot{\mathbf{P}} \mathbf{1}_N = \frac{1}{N} \mathbf{U}_i \mathbf{K}_b \mathbf{1}_N$. Since $\mathbf{K}_b \mathbf{1}_N = \mathbf{0}$, $\dot{\mathbf{g}} = \mathbf{0}$. Assuming the system is initially at rest (i.e., $\dot{\mathbf{g}}(t=0) = \mathbf{0}$), we conclude $\dot{\mathbf{g}} = \mathbf{0} \forall t$. \square

Proposition 3. *The formation variable θ is invariant under \mathbf{U}_γ , \mathbf{U}_g and \mathbf{U}_s .*

Proof. We start with \mathbf{U}_γ . As $\theta = \text{atan}2(h_2, h_1)$, we study the dynamics of h_1 and h_2 . Under \mathbf{U}_γ , $\dot{\mathbf{P}} = \mathbf{U}_\gamma$. From the properties of \mathbf{K}_b , we have $\mathbf{U}_\gamma \mathbf{K}_b = \mathbf{U}_\gamma$ and therefore $\dot{\mathbf{P}}_b = \dot{\mathbf{P}} \mathbf{K}_b = \mathbf{U}_\gamma \mathbf{K}_b = \mathbf{U}_\gamma$. We can then write:

$$\begin{aligned} \ddot{h}_1 &= \left(\text{tr}(\mathbf{P}_{db} \mathbf{P}_{db}^\top) \right)^{-1} \text{tr}(\ddot{\mathbf{P}}_b \mathbf{P}_{db}^\top) = \left(\text{tr}(\mathbf{P}_{db} \mathbf{P}_{db}^\top) \right)^{-1} \text{tr}(\mathbf{U}_\gamma \mathbf{P}_{db}^\top) \\ &= \left(\text{tr}(\mathbf{P}_{db} \mathbf{P}_{db}^\top) \right)^{-1} \text{tr} \left(\alpha_H (k_{1H} (\mathbf{H} \mathbf{P}_{db} \mathbf{P}_{db}^\top - \mathbf{P}_b \mathbf{P}_{db}^\top) \right. \\ &\quad + k_{2H} (\dot{\mathbf{H}} \mathbf{P}_{db} \mathbf{P}_{db}^\top - \dot{\mathbf{P}}_b \mathbf{P}_{db}^\top)) \\ &\quad \left. + \alpha_G (k_{1G} (\mathbf{P}_b \mathbf{P}_{db}^\top (\mathbf{P}_{db} \mathbf{P}_{db}^\top)^{-1} \mathbf{P}_{db} \mathbf{P}_{db}^\top - \mathbf{P}_b \mathbf{P}_{db}^\top) \right. \\ &\quad \left. + k_{2G} (\dot{\mathbf{P}}_b \mathbf{P}_{db}^\top (\mathbf{P}_{db} \mathbf{P}_{db}^\top)^{-1} \mathbf{P}_{db} \mathbf{P}_{db}^\top - \dot{\mathbf{P}}_b \mathbf{P}_{db}^\top)) \right). \end{aligned} \quad (41)$$

Since $(\mathbf{P}_{db} \mathbf{P}_{db}^\top)^{-1} \mathbf{P}_{db} \mathbf{P}_{db}^\top = \mathbf{I}_{2 \times 2}$, the term multiplied by α_G is zero. Besides, it holds that $\text{tr}(\mathbf{P}_b \mathbf{P}_{db}^\top) = \text{tr}(\mathbf{H} \mathbf{P}_{db} \mathbf{P}_{db}^\top)$, as noted above; and, taking the time derivative, $\text{tr}(\dot{\mathbf{P}}_b \mathbf{P}_{db}^\top) = \text{tr}(\dot{\mathbf{H}} \mathbf{P}_{db} \mathbf{P}_{db}^\top)$. If we apply these relations in (41), we get $\ddot{h}_1 = 0$. By following the same procedure for \ddot{h}_2 , we obtain $\ddot{h}_2 = 0$, which yields $\ddot{\mathbf{H}} = \mathbf{0}$. Assuming that the system is at rest at $t = 0$, i.e., $\dot{\mathbf{P}}(t=0) = \mathbf{0}$, we determine that $\dot{\mathbf{H}} = \mathbf{0}$. Hence, θ is invariant under \mathbf{U}_γ .

Under \mathbf{U}_g , $\ddot{\mathbf{P}}_b = \mathbf{U}_g \mathbf{K}_b = -k_{1g} \mathbf{e}_g \mathbf{1}_N^\top \mathbf{K}_b - k_{2g} \dot{\mathbf{P}}_b$. As $\mathbf{1}_N^\top \mathbf{K}_b = \mathbf{0}$, and assuming $\dot{\mathbf{P}}_b(t=0) = \mathbf{0}$, we have $\dot{\mathbf{P}}_b = \mathbf{P}_b = \mathbf{0} \forall t$. Hence, $\dot{\mathbf{H}} = \mathbf{0} \forall t$, and θ is invariant.

Under \mathbf{U}_s , we know from (31) that $\mathbf{H}(t) = \kappa(t) \mathbf{H}(0)$ with $\kappa(t)$ being a scalar. Therefore, h_2/h_1 is constant. If $h_1 = 0$ initially, then $h_1 = 0 \forall t$, and h_2/h_1 is always of infinite magnitude. In conclusion, θ is invariant. \square

Proposition 4. *The formation variable s is invariant under \mathbf{U}_γ and \mathbf{U}_g . It is not invariant under \mathbf{U}_θ .*

Proof. In Proposition 3 we concluded that $\dot{\mathbf{H}} = \mathbf{0}$ under \mathbf{U}_γ and under \mathbf{U}_g . Hence, $s = \|\mathbf{H}\|_2$ is invariant under \mathbf{U}_γ and under \mathbf{U}_g .

Under \mathbf{U}_θ , the third term of (38), which includes \mathbf{SH} , generates the rotation movement. With dynamics of this form, $s = \|\mathbf{H}\|_2$ is not constant in the general case. \square

Remark 1. *The strong invariance properties that we have proven for γ , \mathbf{g} and θ are favorable for achieving a fully uncoupled control. The scale variable s is not invariant under \mathbf{U}_θ (Proposition 4), which creates an undesired coupling that was already expected from the dynamics (18), (19). Despite this, through the use of the term \mathbf{U}_u we will achieve fully uncoupled control of all the variables (γ , \mathbf{g} , θ and s), as shown in the next section.*

IV. STABILITY AND CONVERGENCE UNDER \mathbf{U}

The following is our main formal result, which establishes the stability and convergence of the proposed controller, and provides the dynamics of the variables.

Theorem 1. *The multirobot system under the action of \mathbf{U} (21) is stable and the robot positions \mathbf{P} converge asymptotically to the target configuration \mathbf{P}_T . Moreover, each variable (γ , \mathbf{g} , θ and s) evolves according to linear dynamics uncoupled from the dynamics of the other variables.*

Proof. We will first compute the dynamics imposed by the control law \mathbf{U} (21) for \mathbf{P} , h_1 and h_2 , and then we will use this to obtain the dynamics of the formation variables. We start by computing $\ddot{\mathbf{P}}$:

$$\begin{aligned} \ddot{\mathbf{P}} &= \alpha_H k_{1H} (\mathbf{H} \mathbf{P}_{db} - \mathbf{P}_b) + \alpha_H k_{2H} (\dot{\mathbf{H}} \mathbf{P}_{db} - \dot{\mathbf{P}}_b) \\ &\quad + \alpha_G k_{1G} (\mathbf{G} \mathbf{P}_{db} - \mathbf{P}_b) + \alpha_G k_{2G} (\dot{\mathbf{G}} \mathbf{P}_{db} - \dot{\mathbf{P}}_b) \\ &\quad - k_{1g} \mathbf{e}_g \mathbf{1}_N^\top - k_{2g} \dot{\mathbf{P}} - k_{1s} e_s (1/s) \mathbf{H} \mathbf{P}_{db} - k_{2s} \dot{\mathbf{P}}_b \\ &\quad - k_{1\theta} e_\theta \mathbf{S} \mathbf{H} \mathbf{P}_{db} - k_{2\theta} \dot{\mathbf{P}}_b - \dot{\theta}^2 \mathbf{H} \mathbf{P}_{db} + \frac{2\dot{s}\dot{\theta}}{s} \mathbf{S} \mathbf{H} \mathbf{P}_{db}. \end{aligned} \quad (42)$$

Let us define $k_{2f} = k_{2g} + k_{2s} + k_{2\theta}$ and

$$\eta = k_{1s} \frac{e_s}{s} + \dot{\theta}^2, \quad \rho = k_{1\theta} e_\theta - \frac{2\dot{s}\dot{\theta}}{s}. \quad (43)$$

We then have these expressions for \ddot{h}_1 and \ddot{h}_2 :

$$\begin{aligned} \ddot{h}_1 &= -k_{2g} \dot{h}_1 - k_{1s} (e_s/s) h_1 - k_{2s} \dot{h}_1 + k_{1\theta} e_\theta h_2 - k_{2\theta} \dot{h}_1 \\ &\quad - \dot{\theta}^2 h_1 - \frac{2\dot{s}\dot{\theta}}{s} h_2 = -k_{2f} \dot{h}_1 - \eta h_1 + \rho h_2. \end{aligned} \quad (44)$$

$$\begin{aligned} \ddot{h}_2 &= -k_{2g} \dot{h}_2 - k_{1s} (e_s/s) h_2 - k_{2s} \dot{h}_2 - k_{1\theta} e_\theta h_1 - k_{2\theta} \dot{h}_2 \\ &\quad - \dot{\theta}^2 h_2 + \frac{2\dot{s}\dot{\theta}}{s} h_1 = -k_{2f} \dot{h}_2 - \eta h_2 - \rho h_1. \end{aligned} \quad (45)$$

Recall that the control term \mathbf{U}_γ produces $\ddot{h}_1 = \ddot{h}_2 = 0$, which is why it does not appear in (44) and (45). We can now obtain the error dynamics of each variable.

1) Error dynamics of γ . Note γ itself is an error variable with respect to its desired value $\gamma = \gamma_d = 0$. To analyze γ we will compute the dynamics of the variables \mathbf{E}_γ and \mathbf{E}_{GH} . To this end, we first write the expression for $\ddot{\mathbf{P}}_b$ from (42), using that $\mathbf{1}_N^\top \mathbf{K}_b = \mathbf{0}$:

$$\begin{aligned} \ddot{\mathbf{P}}_b &= \alpha_H k_{1H} (\mathbf{H} \mathbf{P}_{db} - \mathbf{P}_b) + \alpha_H k_{2H} (\dot{\mathbf{H}} \mathbf{P}_{db} - \dot{\mathbf{P}}_b) \\ &\quad + \alpha_G k_{1G} (\mathbf{G} \mathbf{P}_{db} - \mathbf{P}_b) + \alpha_G k_{2G} (\dot{\mathbf{G}} \mathbf{P}_{db} - \dot{\mathbf{P}}_b) \\ &\quad - k_{2f} \dot{\mathbf{P}}_b - \eta \mathbf{H} \mathbf{P}_{db} - \rho \mathbf{S} \mathbf{H} \mathbf{P}_{db}. \end{aligned} \quad (46)$$

We compute from (44) and (45) the dynamics of \mathbf{H} :

$$\ddot{\mathbf{H}} = -k_{2f} \dot{\mathbf{H}} - \eta \mathbf{H} - \rho \mathbf{S} \mathbf{H}. \quad (47)$$

For \mathbf{G} , from (46) and using $\mathbf{P}_{db} \mathbf{P}_{db}^\top = \mathbf{I}_{2 \times 2}$ we obtain

$$\begin{aligned} \ddot{\mathbf{G}} &= \ddot{\mathbf{P}}_b \mathbf{P}_{db}^\top = -k_{2f} \dot{\mathbf{G}} - \alpha_H k_{1H} (\mathbf{G} - \mathbf{H}) \\ &\quad - \alpha_H k_{2H} (\dot{\mathbf{G}} - \dot{\mathbf{H}}) - \eta \mathbf{H} - \rho \mathbf{S} \mathbf{H}. \end{aligned} \quad (48)$$

Notice that

$$\ddot{\mathbf{G}} - \ddot{\mathbf{H}} = -\alpha_H k_{1H} (\mathbf{G} - \mathbf{H}) - (\alpha_H k_{2H} + k_{2f}) (\dot{\mathbf{G}} - \dot{\mathbf{H}}). \quad (49)$$

Now, using $\ddot{\mathbf{P}}_b - \ddot{\mathbf{H}}\mathbf{P}_{db} = \ddot{\mathbf{P}}_b - \ddot{\mathbf{G}}\mathbf{P}_{db} + (\ddot{\mathbf{G}} - \ddot{\mathbf{H}})\mathbf{P}_{db}$, we can directly get, substituting equations (46) to (49):

$$\begin{aligned}\ddot{\mathbf{E}}_\gamma &= \ddot{\mathbf{P}}_b - \ddot{\mathbf{H}}\mathbf{P}_{db} = -(\alpha_H k_{1H} + \alpha_G k_{1G})\mathbf{E}_\gamma \\ &\quad - (\alpha_H k_{2H} + \alpha_G k_{2G} + k_{2f})\dot{\mathbf{E}}_\gamma \\ &\quad + \alpha_G k_{1G}\mathbf{E}_{GH} + \alpha_G k_{2G}\dot{\mathbf{E}}_{GH},\end{aligned}\quad (50)$$

$$\begin{aligned}\ddot{\mathbf{E}}_{GH} &= \ddot{\mathbf{G}}\mathbf{P}_{db} - \ddot{\mathbf{H}}\mathbf{P}_{db} = \\ &\quad - \alpha_H k_{1H}\mathbf{E}_{GH} - (\alpha_H k_{2H} + k_{2f})\dot{\mathbf{E}}_{GH}.\end{aligned}\quad (51)$$

Notice that this forms a linear system for each of the $2N$ components (i.e., position coordinates) of \mathbf{E}_γ and \mathbf{E}_{GH} . Every one of these systems has the same dynamics. Therefore, it suffices to study one of them. Let us take an arbitrary $i \in \{1, \dots, 2N\}$ and call $e_\gamma \in \mathbb{R}$ and $e_{GH} \in \mathbb{R}$ the components of \mathbf{E}_γ and \mathbf{E}_{GH} , respectively, corresponding to that i . We can then write

$$\underbrace{\begin{bmatrix} \dot{e}_\gamma \\ \ddot{e}_\gamma \\ \dot{e}_{GH} \\ \ddot{e}_{GH} \end{bmatrix}}_{\mathbf{A}_e} = \underbrace{\begin{bmatrix} 0 & 1 & 0 & 0 \\ a_{21} & a_{22} & a_{23} & a_{24} \\ 0 & 0 & 0 & 1 \\ 0 & 0 & a_{43} & a_{44} \end{bmatrix}}_{\mathbf{A}_e} \begin{bmatrix} e_\gamma \\ \dot{e}_\gamma \\ e_{GH} \\ \dot{e}_{GH} \end{bmatrix}, \quad (52)$$

where $a_{21} = -(\alpha_H k_{1H} + \alpha_G k_{1G})$, $a_{22} = -(\alpha_H k_{2H} + \alpha_G k_{2G} + k_{2f})$, $a_{23} = \alpha_G k_{1G}$, $a_{24} = \alpha_G k_{2G}$, $a_{43} = -\alpha_H k_{1H}$, $a_{44} = -(\alpha_H k_{2H} + k_{2f})$. We compute the characteristic polynomial of \mathbf{A}_e :

$$|\lambda\mathbf{I} - \mathbf{A}_e| = (\lambda^2 - a_{22}\lambda - a_{21})(\lambda^2 - a_{44}\lambda - a_{43}). \quad (53)$$

As a_{22} , a_{21} , a_{44} and a_{43} are all strictly negative, from the Routh-Hurwitz criterion the eigenvalues of \mathbf{A}_e have negative real parts, and hence the system is stable. Therefore, \mathbf{E}_γ , $\dot{\mathbf{E}}_\gamma$, \mathbf{E}_{GH} and $\dot{\mathbf{E}}_{GH}$ are all bounded and they converge to zero asymptotically. Notice, then, that $\gamma = (1/2)\text{tr}(\mathbf{E}_\gamma^\top \mathbf{E}_\gamma)$ is bounded and converges to zero asymptotically. Moreover, the dynamics of \mathbf{E}_γ are fully determined by the initial configuration and matrix \mathbf{A}_e : therefore, γ does not depend on the other variables being controlled (\mathbf{g} , s , θ).

2) Error dynamics of \mathbf{g} . We substitute (42) in $\ddot{\mathbf{g}} = (1/N)\ddot{\mathbf{P}}\mathbf{1}_N$. Note that every addend ending in a b in (42) is being post-multiplied by \mathbf{K}_b . Then, since $\mathbf{K}_b\mathbf{1}_N = \mathbf{0}$ and $\mathbf{1}_N^\top \mathbf{1}_N = N$, we directly find: $\ddot{\mathbf{g}} = -k_{1g}\mathbf{e}_g - k_{2g}\dot{\mathbf{g}}$. Therefore, we have:

$$\ddot{\mathbf{e}}_g = -k_{1g}\mathbf{e}_g - k_{2g}\dot{\mathbf{e}}_g. \quad (54)$$

We can define $\mathbf{e}_g = [e_{gx}, e_{gy}]^\top$, and then for each component j ($j \in \{x, y\}$) we have a linear system $\dot{\mathbf{x}}_{egj} = \mathbf{A}_g \mathbf{x}_{egj}$ on the state $\mathbf{x}_{egj} = [e_{gj}, \dot{e}_{gj}]^\top$. The characteristic polynomial of \mathbf{A}_g is $\lambda^2 + k_{2g}\lambda + k_{1g}$. As k_{1g} and k_{2g} are positive, from the Routh-Hurwitz criterion \mathbf{e}_g and $\dot{\mathbf{e}}_g$ are bounded and stable, converging to zero over time. Hence, the centroid \mathbf{g} converges to the desired one, \mathbf{g}_d .

3) Error dynamics of s . Substituting (44) and (45) in the second equation of (18) and applying $h_1\dot{h}_1 + h_2\dot{h}_2 = \dot{s}s$ (18) and $h_1^2 + h_2^2 = s^2$, we find $\ddot{s} = -k_{1s}e_s - k_{2f}s$, i.e.:

$$\ddot{e}_s = -k_{1s}e_s - k_{2f}\dot{e}_s. \quad (55)$$

We define a linear system $\dot{\mathbf{x}}_{es} = \mathbf{A}_s \mathbf{x}_{es}$ on the state $\mathbf{x}_{es} = [e_s, \dot{e}_s]^\top$. The characteristic polynomial of \mathbf{A}_s is $\lambda^2 + k_{2f}\lambda + k_{1s}$. As k_{1s} and k_{2f} are positive, from the Routh-Hurwitz criterion e_s and \dot{e}_s are bounded and stable, converging to zero over time. Hence, s converges to the desired scale, s_d .

4) Error dynamics of θ . Substituting (44) and (45) in the second equation of (19) and applying $h_1\dot{h}_2 - h_2\dot{h}_1 = \dot{\theta}s^2$ (19) and $h_1^2 + h_2^2 = s^2$, we find $\ddot{\theta} = -k_{1\theta}e_\theta - k_{2f}\dot{\theta}$, i.e.:

$$\ddot{e}_\theta = -k_{1\theta}e_\theta - k_{2f}\dot{e}_\theta. \quad (56)$$

We now have a linear system $\dot{\mathbf{x}}_{e\theta} = \mathbf{A}_\theta \mathbf{x}_{e\theta}$ on the state $\mathbf{x}_{e\theta} = [e_\theta, \dot{e}_\theta]^\top$. The characteristic polynomial of \mathbf{A}_θ is $\lambda^2 + k_{2f}\lambda + k_{1\theta}$. As $k_{1\theta}$ and k_{2f} are positive, from the Routh-Hurwitz criterion e_θ and \dot{e}_θ are bounded and stable, converging to zero over time. Thus, the angle θ converges to the desired one, θ_d .

Now, from **2), 3) and 4)**, it is clear that the evolutions of \mathbf{g} , s and θ are determined by the initial configuration and the matrices \mathbf{A}_g , \mathbf{A}_s , and \mathbf{A}_θ , respectively, which depend only on the chosen control gains. Hence, during the task each variable evolves independently from the others.

Convergence to the target configuration. Notice from the dynamics above that $\mathbf{P}_b - \mathbf{H}\mathbf{P}_{db}$ and $\dot{\mathbf{P}}_b - \dot{\mathbf{H}}\mathbf{P}_{db}$ are bounded. In addition, s , θ , \dot{s} and $\dot{\theta}$, which represent the value and dynamics of the norm and angle of \mathbf{H} , are also bounded. This implies that \mathbf{P}_b and $\dot{\mathbf{P}}_b$ are bounded. Since \mathbf{g} and $\dot{\mathbf{g}}$ are also bounded, we infer that \mathbf{P} and $\dot{\mathbf{P}}$ are bounded. The convergence is to a static configuration, i.e., $\dot{\mathbf{P}} = \mathbf{0}$. This is because $\dot{\mathbf{H}}$ converges to zero (as \dot{s} and $\dot{\theta}$ converge to zero), and therefore, $\dot{\mathbf{P}}_b = \dot{\mathbf{H}}\mathbf{P}_{db}$ converges to zero. Given that $\dot{\mathbf{g}}$ also converges to zero, $\dot{\mathbf{P}}$ converges to $\mathbf{0}$.

Recall the target configuration is $\mathbf{P}_T = s_d \mathbf{R}_d(\theta_d) \mathbf{P}_{db} + \mathbf{g}_d \mathbf{1}_N^\top$. Let us use a subscript c to denote the configuration that the system converges to, and its variables. This configuration satisfies $\mathbf{P}_c \mathbf{K}_b = \mathbf{H}_c \mathbf{P}_{db}$ (due to $\gamma = 0$), i.e., $\mathbf{P}_c = s_c \mathbf{R}_c \mathbf{P}_{db} + \mathbf{g}_c \mathbf{1}_N^\top$. As $e_s = 0$ and $e_\theta = 0$, we have $s_c = s_d$ and $\theta_c = \theta_d$. As $\mathbf{e}_g = \mathbf{0}$, we have $\mathbf{g}_c = \mathbf{g}_d$. Therefore, $\mathbf{P}_c = \mathbf{P}_T$. \square

Remark 2. As demonstrated above, we can control the time evolutions of γ , \mathbf{g} , s and θ independently. This is another advantage of our new control law with respect to [22]. To avoid overshooting in the transport scenario we consider, we can choose the gains in the overdamped region, i.e., $k_{2j} \geq 2\sqrt{k_{1j}}$, for $j \in \{H, G, g\}$. In the case of s and θ , their dynamics share the coefficient k_{2f} as seen in (55)-(56), so we can fix k_{2f} and then define $k_{1s} \leq k_{2f}^2/4$, $k_{1\theta} \leq k_{2f}^2/4$. Note that the actual time evolutions of the variables are also determined by the safety constraints imposed via the CBFs.

V. EXPERIMENTAL VALIDATION

A. Simulation results

We test the uncoupling properties in four scenarios (see Fig. 1), with $N = 6$ robots manipulating a squared sheet modelled in 3D with mass-spring-damper elements of 0.5 [N·s/m] damping, 0.025 [kg] nodal mass, and varying stiffness. CBFs are not used in these tests. We choose $k_{1H} = 0.2$, $k_{2H} = 0.5$, $k_{1G} = 0.2$, $k_{2G} = 0.5$, $\alpha_H = 1$, $\alpha_G = 10$, $k_{1s} = 2$, $k_{2s} = 4$, $k_{1g} = 0.2$, $k_{2g} = 1$, $k_{1\theta} = 2$, $k_{2\theta} = 4$,

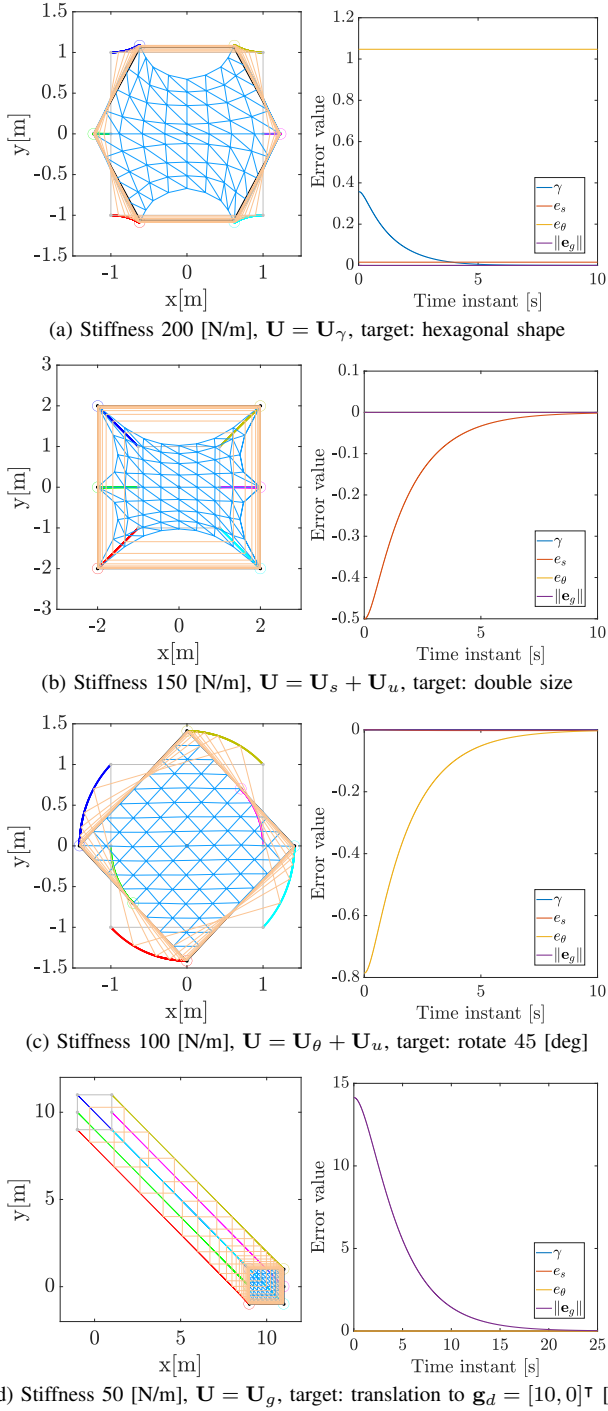


Fig. 1. Simulation results to illustrate the uncoupling properties of the controller. Left column: final top-view snapshots, with the object shown as a blue mesh, and robot team paths. Right column: error plots.

$s_d = 1$, $\theta_d = 0$, and the control time step is 0.01 [s]. The motions are efficient, and fully uncoupled, as expected from our analysis: only the controlled variable changes in each case. The shape of the sheet evolves suitably and undesired deformations are avoided. There is an almost imperceptible drift in e_s in case (c) ($e_s = -2.3 \cdot 10^{-3}$ at $t = 10$ [s]), due to the discrete-time implementation of the rotation control.

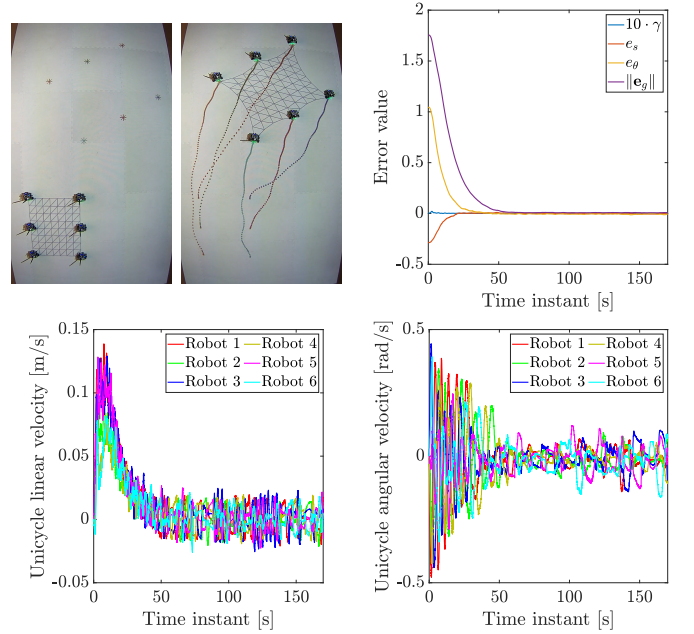


Fig. 2. From left to right and top to bottom: top view (rotated 90 [deg]) of the scenario at $t = 0$, 165 [s]; control errors; unicycle linear velocities; and unicycle angular velocities. In the two first plots, a large deformable object is transported and deformed from the rectangular formation seen in the first image to a scaled and rotated rectangle seen at the top of the second image.

B. Experimental results

The performance of the proposed controller in real scenarios is tested with and without obstacles in the Robotarium [23]. Since the robots follow unicycle kinematics, we integrate the acceleration values and then transform the resulting velocities to the unicycle model by means of a diffeomorphism. In the first test, illustrated in Fig. 2, a 0.6×0.75 [m] deformable virtual sheet modelled in 3D with ARAP [13], is transported by a formation of $N = 6$ robots. The goal configuration is a rectangle with $\mathbf{g}_d = [-0.75, 0.15]^\top$ [m] (the origin of coordinates is at the center of the arena), $s_d = 1$ and $\theta_d = 0$ [rad]. We configure the parameters in the overdamped region (Remark 2): $k_{1H} = 0.1$, $k_{2H} = 0.65$, $k_{1G} = 0.1$, $k_{2G} = 0.65$, $\alpha_H = 4$, $\alpha_G = 2$, $k_{1s} = 0.1$, $k_{2s} = 0.3$, $k_{1g} = 0.02$, $k_{2g} = 0.3$, $k_{1\theta} = 0.1$, $k_{2\theta} = 0.3$ and the control time step is 0.033 [s]. \mathbf{P}_T is reached with near-zero errors, despite the noise and perturbations from the real setup (control input conversion, measurement/actuation errors, etc). It is also interesting to see that our controller is applicable on unicycles. CBFs were not used in this test.

In the second test, shown in Fig. 3, a rectangular deformable sheet also modelled with ARAP is transported to a deformed configuration avoiding collision with obstacles. The sheet of 0.45×0.56 [m] is grasped by four robots at its corners and transported to the target configuration defined as a trapezoid with $\mathbf{g}_d = [-0.8, 0.25]^\top$ [m], $s_d = 1$ and $\theta_d = 0$ [rad]. We consider two obstacles (one static, one dynamic). Following [11], [22], for further safety, we circumscribe obstacles and take the resulting circle as the borderline for collision avoidance. The radius of the obstacles is 0.16 [m]. We configure the controller \mathbf{U} with the same parameters as in the previous case, except for $k_{1g} = 0.01$. The system

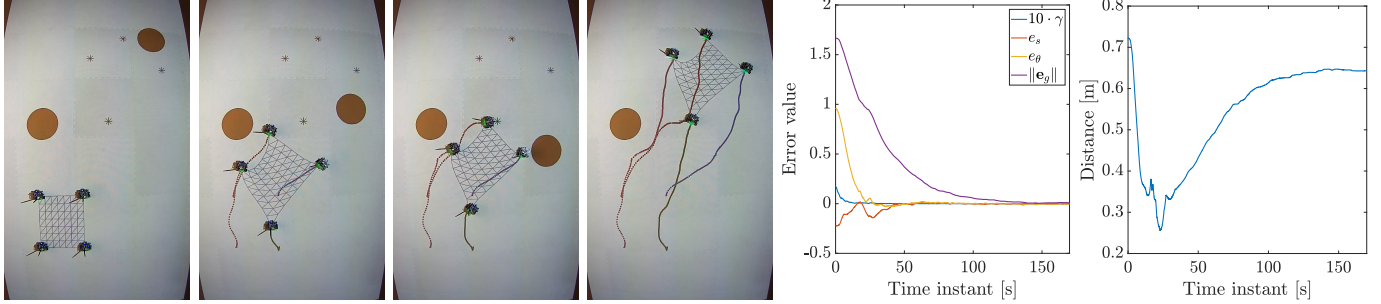


Fig. 3. From left to right: top-view snapshots (rotated 90 [deg]) at $t = 0, 15, 22, 165$ [s] of the second test, with one static and one dynamic obstacles; control errors; and minimum distances between the mesh nodes and the nearest obstacle. It can be seen that the errors evolve to a stationary near-zero value. The minimum distances are always above 0.16 [m], the radius of the obstacles, i.e., no collisions occur between the object and the obstacles.

we propose does not consider explicitly collision avoidance in the formulation, so we use the method in [22, Sect. IV] to augment \mathbf{U} with CBFs. These CBFs provide a robust collision avoidance behaviour that acts locally, when obstacles approach, by minimally modifying the nominal control input. They also prevent overstretching during collision avoidance maneuvers. The control task is successfully completed with a low computation time per cycle including CBFs (4 [ms] on an i7 3.2GHz CPU) which is suitable for usual scenarios. We provide additional results in the attached video.

VI. CONCLUSION

Our new formation controller allows steering a deformable object to a specific configuration in 2D by means of a team of robots assuming that the deformable object's shape adapts to the shape of the robotic formation. The controller includes different terms that modify the shape, scale, position and orientation of the robotic formation. We have demonstrated theoretically the uncoupling between the variables and the stability and convergence of the system under our controller. The performance of the system has shown successful results in simulated and real scenarios, without and with obstacles. Using compliant grippers, applying force control in active robot-object links and augmenting our controller with path planning techniques are interesting options for extending the applicability to more complex deformable objects and manipulation scenarios. Another future direction is adapting the controller to other robotic platforms, e.g., quadrotors or Ackermann drive robots.

REFERENCES

- [1] H. Yin, A. Varava, and D. Kragic, "Modeling, learning, perception, and control methods for deformable object manipulation," *Sci. Robot.*, vol. 6, no. 54, p. eabd8803, 2021.
- [2] Z. Feng, G. Hu, Y. Sun, and J. Soon, "An overview of collaborative robotic manipulation in multi-robot systems," *Annu. Rev. Control*, vol. 49, pp. 113–127, 2020.
- [3] R. Herguedas, G. Lopez-Nicolas, R. Aragues, and C. Sagüés, "Survey on multi-robot manipulation of deformable objects," in *Proc. IEEE Int. Conf. Emerg. Technol. Fact. Autom.*, 2019, pp. 977–984.
- [4] M. Aranda, J. Sanchez, J. A. Corrales Ramon, and Y. Mezouar, "Robotic motion coordination based on a geometric deformation measure," *IEEE Syst. J.*, vol. 16, no. 3, pp. 3689–3699, 2022.
- [5] P. C. Lusk, X. Cai, S. Wadhwania, A. Paris, K. Fathian, and J. P. How, "A Distributed Pipeline for Scalable, Deconflicted Formation Flying," *IEEE Robot. Automat. Lett.*, vol. 5, no. 4, pp. 5213–5220, 2020.
- [6] Z. Lin, L. Wang, Z. Chen, M. Fu, and Z. Han, "Necessary and sufficient graphical conditions for affine formation control," *IEEE Trans. Automat. Control*, vol. 61, no. 10, pp. 2877–2891, 2016.
- [7] K. Fathian, T. H. Summers, and N. R. Gans, "Robust distributed formation control of agents with higher-order dynamics," *IEEE Control Syst. Lett.*, vol. 2, no. 3, pp. 495–500, 2018.
- [8] S. Zhao, "Affine formation maneuver control of multiagent systems," *IEEE Trans. Automat. Control*, vol. 63, no. 12, pp. 4140–4155, 2018.
- [9] S. Zhao, D. V. Dimarogonas, Z. Sun, and D. Bauso, "A general approach to coordination control of mobile agents with motion constraints," *IEEE Trans. Automat. Control*, vol. 63, no. 5, pp. 1509–1516, 2018.
- [10] A. D. Ames, S. Coogan, M. Egerstedt, G. Notomista, K. Sreenath, and P. Tabuada, "Control Barrier Functions: Theory and Applications," in *Proc. Eur. Control Conf.*, 2019, pp. 3420–3431.
- [11] L. Wang, A. D. Ames, and M. Egerstedt, "Safety Barrier Certificates for Collisions-Free Multirobot Systems," *IEEE Trans. Robot.*, vol. 33, no. 3, pp. 661–674, 2017.
- [12] W. S. Cortez, D. Oetomo, C. Manzie, and P. Choong, "Control Barrier Functions for Mechanical Systems: Theory and Application to Robotic Grasping," *IEEE Trans. Control Syst. Technol.*, vol. 29, no. 2, pp. 530–545, 2021.
- [13] O. Sorkine and M. Alexa, "As-Rigid-as-Possible surface modeling," in *Proc. Eurographics Symp. Geometry Process.*, 2007, pp. 109–116.
- [14] M. Shetab-Bushehri, M. Aranda, Y. Mezouar, and E. Ozgur, "As-Rigid-as-Possible Shape Servoing," *IEEE Robot. Automat. Lett.*, vol. 7, no. 2, pp. 3898–3905, 2022.
- [15] J. Alonso-Mora, R. Knepper, R. Siegwart, and D. Rus, "Local motion planning for collaborative multi-robot manipulation of deformable objects," in *Proc. IEEE Int. Conf. Robot. Autom.*, 2015, pp. 5495–5502.
- [16] C. Yang, G. N. Sue, Z. Li, L. Yang, H. Shen, Y. Chi, A. Rai, J. Zeng, and K. Sreenath, "Collaborative navigation and manipulation of a cable-towed load by multiple quadrupedal robots," *IEEE Robot. Automat. Lett.*, vol. 7, no. 4, pp. 10 041–10 048, 2022.
- [17] D. McConachie, A. Dobson, M. Ruan, and D. Berenson, "Manipulating deformable objects by interleaving prediction, planning, and control," *Int. J. Robot. Res.*, vol. 39, no. 8, pp. 957–982, 2020.
- [18] J. Hu, W. Liu, H. Zhang, J. Yi, and Z. Xiong, "Multi-Robot Object Transport Motion Planning With a Deformable Sheet," *IEEE Robot. Automat. Lett.*, vol. 7, no. 4, pp. 9350–9357, 2022.
- [19] K. Hunte and J. Yi, "Pose Control of a Spherical Object Held by Deformable Sheet with Multiple Robots," *IFAC-PapersOnLine*, vol. 55, no. 37, pp. 414–419, 2022.
- [20] G. Lopez-Nicolas, R. Herguedas, M. Aranda, and Y. Mezouar, "Simultaneous shape control and transport with multiple robots," in *Proc. IEEE Int. Conf. Robotic Comp.*, 2020, pp. 218–225.
- [21] R. Herguedas, G. López-Nicolás, and C. Sagüés, "Multirobot Transport of Deformable Objects With Collision Avoidance," *IEEE Syst. J.*, vol. 17, no. 2, pp. 3224–3234, 2023.
- [22] R. Herguedas, M. Aranda, G. Lopez-Nicolas, C. Sagüés, and Y. Mezouar, "Multirobot control with double-integrator dynamics and control barrier functions for deformable object transport," in *Proc. IEEE Int. Conf. Robot. Autom.*, 2022, pp. 1485–1491.
- [23] S. Wilson, P. Glotfelter, L. Wang, S. Mayya, G. Notomista, M. Mote, and M. Egerstedt, "The Robotarium: Globally impactful opportunities, challenges, and lessons learned in remote-access, distributed control of multirobot systems," *IEEE Control Syst. Mag.*, vol. 40, no. 1, pp. 26–44, 2020.